Applied Catalysis B: Environmental 158–159 (2014) 140–149

Contents lists available at ScienceDirect

Applied Catalysis B: Environmental

journal homepage: www.elsevier.com/locate/apcatb

Effect of nitrogen-containing functionalization on the electrocatalytic activity of PtRu nanoparticles supported on carbon nanotubes for direct methanol fuel cells

Yi Cheng [a], Changwei Xu [a,b], Pei Kang Shen [c], San Ping Jiang [a,*]

[a] Fuels and Energy Technology Institute & Department of Chemical Engineering, Curtin University, Perth, WA 6102, Australia
[b] School of Chemistry and Chemical Engineering, Guangzhou University, Guangzhou 510006, China
[c] Advanced Energy Materials Research Laboratory, Sun Yat-sen University, Guangzhou 510275, China

ARTICLE INFO

Article history:
Received 19 December 2013
Received in revised form 1 April 2014
Accepted 8 April 2014
Available online 18 April 2014

Keywords:
Fuel cells
PtRu nanoparticles
Polyelectrolyte
Solvent
Nitrogen-containing functionalization
Methanol oxidation reaction

ABSTRACT

PtRu nanoparticles (NPs) with average size of ~3 nm are supported onto poly(diallyldimethylammonium chloride) (PDDA), polyethylenimine (PEI), 1-aminopyrene (1-AP or AP), and terahydrofuran (THF) functionalized multi-walled carbon nanotubes (CNTs) using microwave assisted self-assembly method. The PtRu/CNTs catalysts are extensively characterized by TGA, TEM, XRD, XPS, cyclic voltammetry and chronoamperometry. Non-covalent functionalization substantially improves the dispersion and distribution of PtRu NPs on CNTs. Most important, the results demonstrate that nitrogen-containing functional groups of the functionalization agents play a critical role in the electrocatalystic activity of PtRu NPs supported on CNTs. PtRu NPs supported on PEI, AP and in less extent PDDA functionalized CNTs exhibited significantly higher electrocatalystic activity and stability for the electro-oxidation of methanol as compared with PtRu supported on THF-CNTs and conventional acid-treated CNTs. The superior activity of PtRu supported on functionalized CNTs is most likely due to the strong interaction of the electron rich nitrogen-containing functional groups of the functionalization agents such as PEI, AP and in less extend PDDA and the PtRu NPs assembled on CNTs.

1. Introduction

Fuel cells are electrochemical devices to directly convert the chemical energy of fuels such as hydrogen, methanol, ethanol, etc. to electricity with high efficiency and low greenhouse gas emission as compared to the conventional energy conversion technologies such as internal combustion engines. Thus fuel cells are expected to play a key role in our future energy economy due to the limited fossil fuel reserves and the increasing energy demand. Direct methanol fuel cell (DMFC), a device anticipated to serve as a power source for mobile application, has been extensively studied due to its advantages, such as high energy density (energy density of methanol is 17,900 kJ/L), relatively quick start-up, rapid response to varying loading, and safe for storage and transportation [1,2]. However, the sluggish kinetics for the methanol oxidation reaction (MOR) inhibit the large-scale production of cost-effective and highly efficient DMFCs [1]. Intensified researches have been conducted all over the world to develop active and stable electrocatalysts for methanol oxidation, particularly in the area of binary alloy catalysts, such as PtRu [3–5], Pt-Os [6], Pt-Sn [7], Pt-W [6] and Pt-Mo [8]. Among these, the PtRu alloy catalyst system is widely accepted as one of the most promising anode catalysts for DMFC [5,9–11]. In order to enhance the dispersion of metal nanoparticles (NPs) and thus to increase the utilization and efficiency of the precious metal, PtRu alloy supported onto high surface area carbon supports, including carbon blacks, mesoporous carbon [12], carbon nanofibers [13], and carbon nanotubes (CNTs) [14], were investigated. Particularly, CNTs have received wide attention as effective catalysts support in fuel cell due to their large specific surface area, high electronic conductivity, and excellent chemical stability [15–17].

Owing to the chemical inert of pristine CNTs, homogenous binding sites need to be introduced onto the surface of the CNTs through surface-functionalization in order to obtain high dispersion of metal NPs on CNTs. The most common covalent functionalization is via the aggressive oxidation treatment in a mixture of HNO_3/H_2SO_4 solution, introducing the carbonyl groups (–COOH) onto the surface of CNTs [18–20]. However, the acid oxidation method inevitably causes some structural damage of CNTs and introduces large amount of defects, consequently

* Corresponding author. Tel.: +61 8 9266 9804; fax: +61 8 9266 1138.
E-mail addresses: stsspk@mail.sysu.edu.cn (P.K. Shen), s.jiang@curtin.edu.au (S.P. Jiang).

http://dx.doi.org/10.1016/j.apcatb.2014.04.017
0926-3373/

disrupting the delocalized electron system and resulting in the loss of their electronic conductivity and corrosion resistance [2,21]. Non-covalent functionalization of CNTs by surfactants [2,21], aromatic compounds [22], polymers or polyelectrolytes [21,23–27] and biomolecules [28] has attracted great interest due to the advantages of providing high density of anchoring site without damage the intrinsic properties of CNTs. A variety of polyelectrolyte and solvents such as poly(diallyldimethylammonium chloride) (PDDA) [29,30], polypyrrole (PPY) [31,32], polyethylenimine (PEI) [25,33], polyaniline (PANI) [26], phenanthroline [34], hydroxyquinoline [7], 1-aminopyrene (1-AP or AP) [22], tetrahydrofuran (THF) [35], have been employed to functionalize CNTs as catalysts supports. Non-covalent fuctionalization by polyelectrolytes and solvent significantly improves the distribution and electrocatalytic activity of Pt and Pt based alloy NPs on CNTs and graphene [7,23,26,29,30,34,36]. The electrocatalystic activity of Pt NPs is also affected by the nature of non-covalent functionalization. We investigated the effect of polyelectrolytes on the electronic structure of Pt NPs on polyelectrolyte functionalized on CNTs [37]. The spectroscopic and electrochemical characterization as well as DFT calculation revealed that polyanions with electron-rich functional groups would donate electrons to Pt atoms which cause an increase in the electron density around Pt atoms and downshift d-band center of Pt, resulting in a weaker chemisorptions of oxygen-containing species (e.g., CO) and enhancing the electrocatalystic activity of Pt NPs [37].

It is of significant importance to understand the influence of the polyelectrolyte and/or solvent on the morphology, distribution and electrocatalytic activity of the Pt-based NPs supported on CNTs in order to develop better and more efficient catalysts for fuel cells. Here, polymers such as PDDA and PEI, and solvents such as AP and THF were selected to functionalize the CNTs as supports for PtRu NPs. PDDA is water-soluble quaternary ammonium strong cationic polyelectrolyte while PEI is one of the most popular amino-rich highly hydrophilic cationic polyelectrolyte for fuel cell applications [25,35,38,39]. AP and THF have been shown to be effective in functionalization of CNTs [22,35,40]. The results clearly indicate that the electrocatalystic activity depends strongly on the composition and structure of the functionalization agents and functionalization agents with ammonium or amino groups are particularly effective to enhance the activity of the PtRu NPs for the methanol oxidation reaction of fuel cells.

2. Experimental

2.1. Functionalization of CNTs

Materials used in this experiment include sulfuric acid (99.5%, Fluka), nitric acid (65%, Fluka), ethanol (Sigma-Aldrich), methanol (Sigma-Aldrich), CNTs (multi-walled CNTs, Shenzhen Nano, China), hexachloroplatinic(IV) acid (Sigma-Aldrich), ruthenium chloride (Sigma-Aldrich), ethylene glycol (Sigma-Aldrich), Nafion solution (5% in isoproponal and water), poly(diallyldimethylammonium chloride) (PDDA, molecular weight over 100,000), polyethylenimine (PEI, molecular weight ~1300, Sigma-Aldrich), 1-aminopyrene (1-AP or AP, molecular weight 217, Sigma-Aldrich), tetrahydrofuran (THF, molecular weight 72, Sigma-Aldrich). All chemicals were used without further purification. Fig. 1 shows the structure of the functionalization agents used in the present study.

CNTs functionalized by PDDA and PEI were synthesized as follow: 200 mg pristine CNTs were ultrasonicated in 400 mL ultrapure water (resistivity 18.2 MΩ cm) for 1 h in presence of 0.5 wt% PDDA or PEI and stirred overnight. During the PDDA functionalization process, 2 g NaCl was added in order to promote

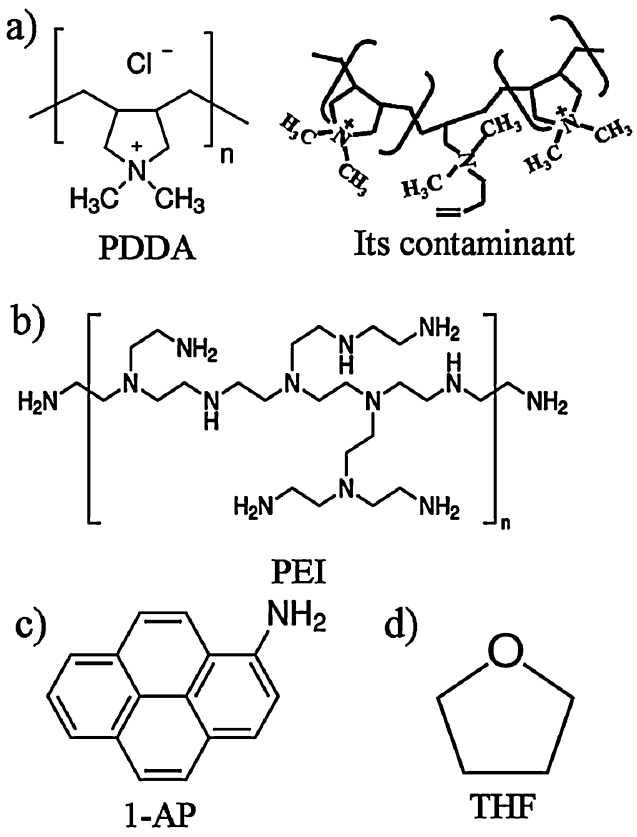

Fig. 1. Molecular structure of functionalization agents used in the present study.

the PDDA functionalization [23,25]. The functionalized CNTs were washed with ultrapure water for several times to remove the excess PDDA or PEI. The products were noted as PDDA-CNTs and PEI-CNTs, respectively. For AP functionalization, 200 mg pristine CNTs and 20 mg AP were ultrasonicated in 100 mL ethanol for 1 h, stirred overnight and filtrated using nylon membrane. This was followed by washing for several times with ethanol to remove the excess AP. The product was denoted as AP-CNTs. In the case of THF functionalization, 200 mg of pristine CNTs were dispersed in 100 mL THF under ultrasonic treatment for 1 h, stirred overnight and filtrated using nylon membrane. The product was noted as THF-CNTs. For comparison, CNTs were also functionalized by a conventional acid oxidation treatment following the procedure reported elsewhere [20]. In this method, 200 mg of CNTs were treated in 200 mL of a mixed acid solution (H_2SO_4:HNO_3 in 1:1 v/v), followed by refluxing at 140 °C for 4 h. The obtained solution was then diluted with 2 L of deionized water to reduce the acidity of the solution, followed by filtration. The acid-treated CNTs were denoted as AO-CNTs. The as-functionalized CNTs were dried in vacuum oven at 70 °C for 24 h.

2.2. Synthesis of PtRu/CNTs electrocatalysts

To prepare PtRu/CNTs, 30 mg PDDA, PEI, AP and THF functionalized CNTs and AO-CNTs were firstly ultrasonicated in 50 mL ethylene glycol (EG) solution for 30 min before the addition of approximate amount of H_2PtCl_6 and $RuCl_3$ with Pt:Ru ratio of 1:1. The solution was controlled at a pH of slightly less than 7 (e.g., pH 6.5) to maintain a weak acidity. The beaker was then placed in a microwave oven and heated for 2 min, followed by stirring overnight under pH 3–4. The solution was then filtered using a nylon filter membrane and washed for several times. The obtained catalysts were dried in a vacuum oven at 70 °C for 24 h. The metal loading on CNTs was controlled at 40 wt%. The products

were denoted as PtRu/PDDA-CNTs, PtRu/PEI-CNTs, PtRu/AP-CNTs, PtRu/THF-CNTs and PtRu/AO-CNTs.

2.3. Characterization

Thermo gravimetric (Q5000, USA) analyses were performed to investigate the thermal stability of functionalized CNTs, the loading of PDDA, PEI, AP and THF, as well as PtRu loading in air. TGA was in equilibrium at 100 °C for 15 min, followed by a ramp of 10 °C min^{-1} up to 800 °C. The Raman spectra were recorded in air at room temperature using a Perkin–Elmer GX Raman spectrometer with a back-scattered configuration and equipped with a Nd:YAG laser at 1064 nm as its light source for Raman. Distributions of PtRu NPs on MWCNT were characterized using a transmission electron microscope (JEOL JEM-2000EX, Japan) operated at 200 kV. Here, the mean sizes of the PtRu NPs were obtained by measuring 250 randomly chosen particles in the TEM images. The products were identified with X-ray diffractometer (XRD, Rigaku D/MAX RINT 2500) operated at 40 kV and 30 mA with Cu Ka (l = 1.5406 Å) in the range of 20–90°. The X-ray photoelectron spectroscopy (XPS) measurements were carried out on a XPS apparatus (ESCALAB 250, Thermo-VG Scientific Ltd.). The Pt:Ru ratio of as obtained catalysts was further confirmed by Inductively Coupled Plasma (ICP-OES, IRIS Intrepid II XSP, USA). The solution for ICP analysis were prepared as follow: the PtRu catalysts were burned in a TG pan, and the solid were collected and digested in a PTFE digestion tank using microwave dissolver (SINEO, HDS-8G) with 10 mL aqua regia (the procedure was set as: 150 °C, 5 min; 180 °C, 5 min; 200 °C, 10 min; 230 °C, 20 min).

The electrochemical measurements were conducted in a standard electrochemical cell using a Princeton potentiostat (Versastat3, USA). Generally, 4 mg of the catalyst was ultrasonically mixed in 4 mL of Nafion solution to form a homogeneous ink, followed by pipetting 10 μL of the catalyst ink onto the surface of a glass carbon electrode (GCE). The diameter of GCE was 4 mm. Pt foil (3.0 cm^2) and Ag/AgCl (saturated KCl) electrodes were used as the counter and reference electrodes, respectively. The electrochemical active area of PtRu/CNTs were measured in a nitrogen-saturated 0.5 M H_2SO_4 solution at a scan rate of 50 mV s^{-1} and the elelctrocatalytic activity for the methanol oxidation reaction was measured in a nitrogen-saturated 0.5 M H_2SO_4 + 1.0 M CH_3OH solution at a scan rate of 50 mV s^{-1}. The cyclic voltammetry (CV) curves were obtained at steady state, i.e., typically after 10–15 cycles. The Pt metal loading was kept at 2 μg. The tests were conducted at 25 °C.

The CO-stripping was performed in a nitrogen-saturated 0.5 M H_2SO_4 solution. First, the solution was bubbled with ultrapure N_2 for 15 min, then CO was introduced by flowing 0.5% CO in N_2 at a flow rate of 50 mL min^{-1} through the working electrode compartment by keeping the potential at −0.12 V versus Ag/AgCl reference electrode for 30 min, followed by bubbling N_2 for 30 min at the same potential. The potential was scanned from 0 to 1.0 V at a scan rate of 50 mV s^{-1}.

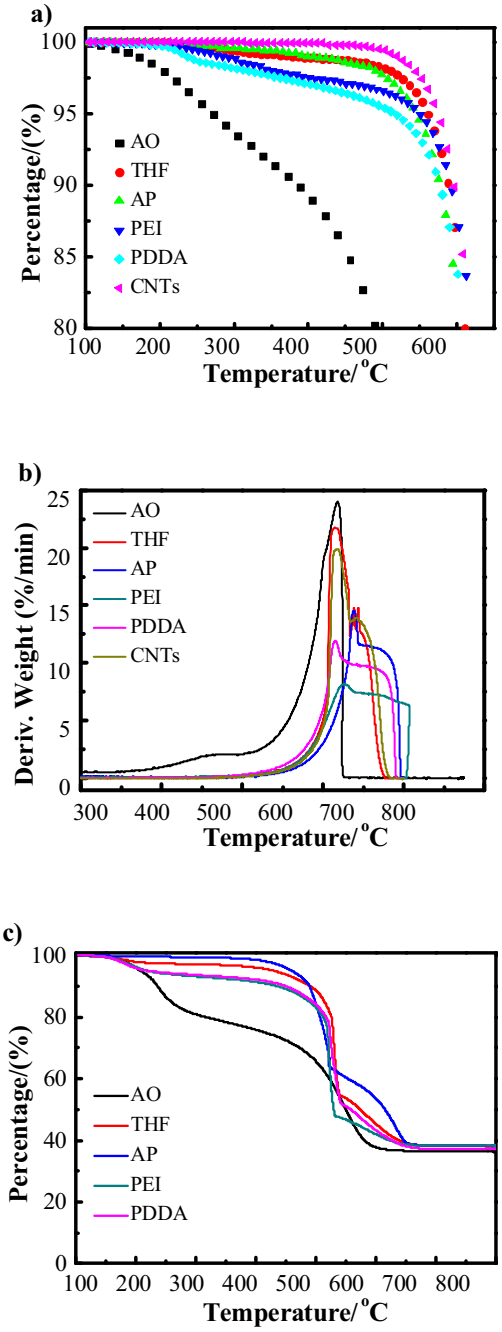

Fig. 2. TGA curves of (a) CNTs, PDDA-CNTs, PEI-CNTs, AP-CNTs, THF-CNTs and AO-CNTs, (b) differential TGA curves, showing the oxidation and decomposition of CNTs and functionalized CNTs, (c) PtRu supported on PDDA-CNTs, PEI-CNTs, AP-CNTs, THF-CNTs and AO-CNTs.

3. Results and discussion

3.1. TGA and Raman spectra analysis of functionalized CNTs

The loadings of PDDA, PEI, AP and THF on CNTs and PtRu on functionalized CNTs were analyzed by TGA method and the results are shown in Fig. 2. The loading of the functionalization agents was determined from the weight loss around 300 °C. The loading of PDDA and PEI on CNTs is 3.5 wt% and 3.0 wt%, respectively, and it is ~1 wt% AP and THF assembled onto CNTs (Fig. 2a). The low loading of AP and THF is probably due to their much smaller molecule weight. The oxidation or decomposition temperature of CNTs is also affected by the functionalization. The decomposition temperatures of PDDA, PEI and AP functionalized CNTs are around 550–690, 550–705, 550–695 °C, respectively, higher than 550–680 °C of pristine CNT (Fig. 2b). This indicates that PDDA, PEI and AP wrapped on CNTs surface improve the thermal stability of CNTs. On the other hand, the decomposition of THF-CNTs slightly shifts to lower temperature (550–670 °C) as compared to that of pristine CNTs. This may be because of the extra oxygen atoms assembled on the surface of CNTs by THF functionalization (Fig. 1). AO-CNTs starts to lose weight at temperatures as low as 200 °C and its decomposition temperature is around 400–620 °C, significantly lower than pristine CNTs. This indicates that acid oxidation treatment reduces

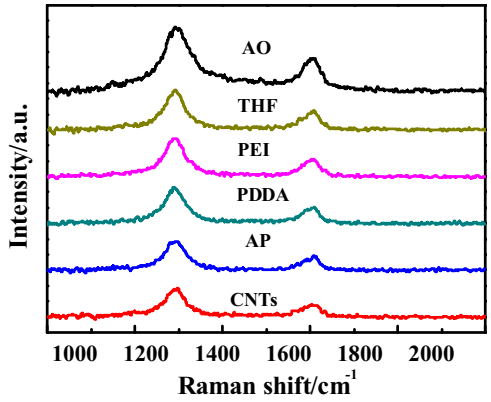

Fig. 3. Raman spectroscopy of pristine CNTs, PDDA-CNTs, PEI-CNTs, AP-CNTs, THF-CNTs and AO-CNTs.

the thermal stability of CNTs probably due to the structural damage of CNTs by acid treatment.

The loading of PtRu NPs on CNTs was also obtained from TGA (Fig. 2c). The PtRu loading supported on PDDA-CNTs, PEI-CNTs, AP-CNTs, THF-CNTs and AO-CNTs is 37.0, 37.1, 38.0, 38.0 and 36.1 wt%, respectively. The measured PtRu loading is close to the targeted loading 40 wt%. The PtRu ratios of as-synthesized catalysts were also analyzed by ICP, and the Pt:Ru ratio supported on PDDA-CNTs, PEI-CNTs, AP-CNTs and THF-CNTs is 0.94:1, 1.01:1, 1.02:1 and 0.97:1, respectively. The loading of functionalization agents, PtRu NPs and decomposition temperature of functionalized CNTs are summarized in Table 1.

Fig. 3 is the Raman spectra of the pristine CNTs and functionalized CNTs. The relative intensity ratio of the D (near 1300 cm^{-1}) to G (in the 1580–1600 cm^{-1} region) band (I_D/I_G) is used as probes of CNT wall integrity (Table 1)[41]. The calculated I_D/I_G value for pristine CNTs is 3.1. For AO-CNTs, the I_D/I_G ratio is 3.6, higher than that of pristine CNTs. This demonstrates that acid oxidation treatment increases the number of defects on the surface of CNTs, resulting in an increase of disordered sp^2 carbon material [42,43]. The values of I_D/I_G of PDDA, PEI, AP and THF functionalized CNTs are 2.85, 2.9, 2.7 and 3.1, respectively, comparable to 3.1 for the pristine CNTs. The results indicate that PDDA, PEI, AP and THF functionalization has no detrimental effects on the integrity of the CNTs. The I_D/I_G ratio of THF-CNTs is almost the same as pristine CNTs and the reason is most likely related to the weak interaction between THF and CNTs. The reduced I_D/I_G ratios of PDDA, PEI and AP functionalized CNTs appears to be consistent with the thermal stability of the corresponding functionalized CNTs.

3.2. TEM, XRD and XPS analysis of PtRu/CNTs catalysts

Fig. 4 shows the TEM images and the corresponding histograms of the particle size distribution of PtRu NPs on functionalized CNTs. In the case of PtRu/AO-CNTs, the dispersion of PtRu NPs is relatively poor with a large number of aggregates and the average particle size of PtRu NPs is ~4.2 nm (Fig. 4e). In the case of PtRu NPs supported on PDDA-CNTs, PEI-CNTs, AP-CNTs and THF-CNTs, the distribution of PtRu NPs is significantly better than that supported on AO-CNTs. The average particle sizes of PtRu NPs supported on PDDA-CNTs, PEI-CNTs, AP-CNTs and THF-CNTs are ~3.13, ~2.98, ~2.94 and ~3.28 nm (Fig. 3a–d), respectively. PDDA, PEI, AP and THF functionalized CNTs are far more effective catalyst supports for Pt-based NPs as compared to the conventional acid-oxidized CNTs.

The morphology and particle size distribution of PtRu NPs appears to be affected by the functionalization agents. The PtRu NPs supported on PEI-CNTs, AP-CNTs and THF-CNTs show better

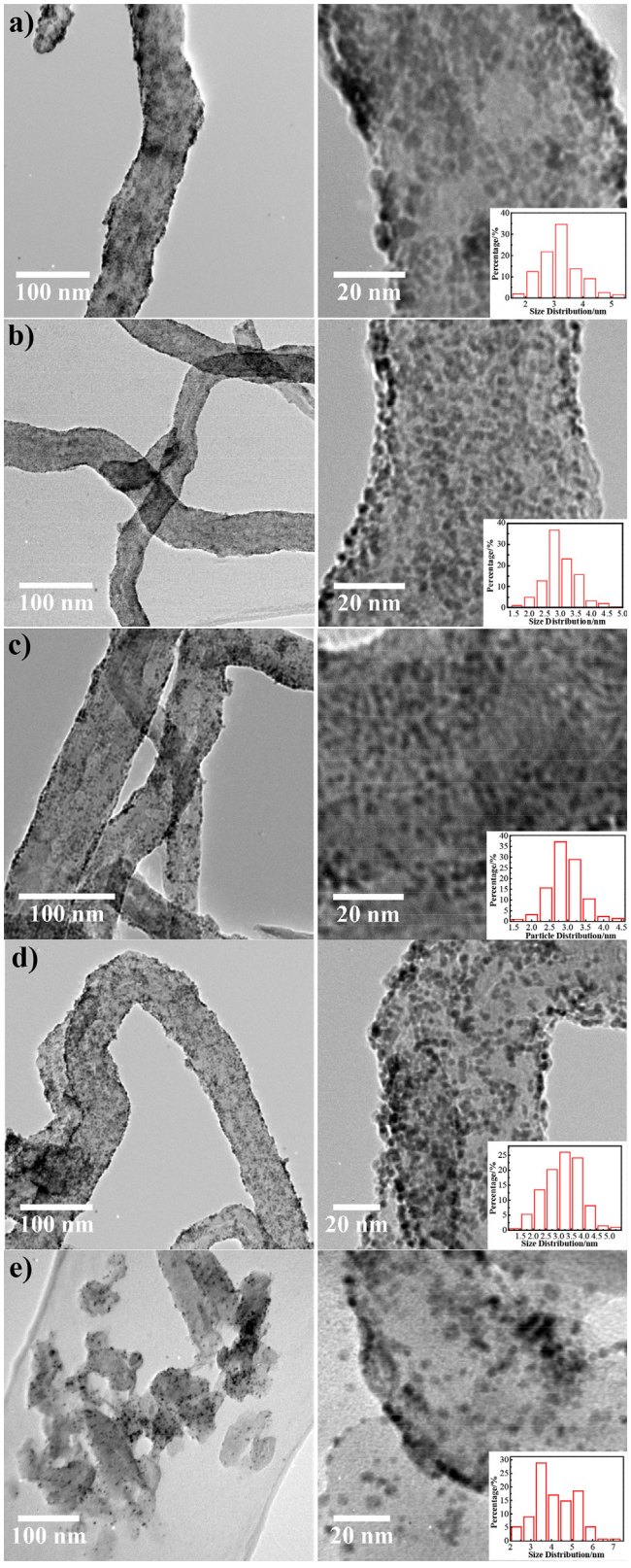

Fig. 4. TEM images of (a) PtRu/PDDA-CNTs, (b) PtRu/PEI-CNTs, (c) PtRu/AP-CNTs, (d) PtRu/THF-CNTs and (e) PtRu/AO-CNTs. Left image is the low magnification TEM and right image is the corresponding high resolution TEM. The inset is the histograms of particle size distribution.

Table 1
TGA and Raman results of PtRu NPs supported on functionalized CNTs.

Functionalized CNTs	Electrolyte loading (%)	PtRu loading (%)	Decomposition temperature (°C)	Raman I_D/I_G
PDDA	3.5	37.0	550–690	2.9
PEI	3.0	37.1	550–705	2.9
AP	1.0	38.0	550–695	2.7
THF	1.0	38.0	550–670	3.1
AO	–	36.1	400–620	3.6
CNTs	–	–	550–680	3.1

dispersion as compared to that on PDDA-CNTs. PDDA used in the present study has a high molecular weight around 100,000, and can interact with the CNTs surface through π–π interaction due to the presence of unsaturated contaminant in the PDDA chain through aligned configuration, helical wrapping, and peseudohelical organization [44,45]. The presence of 2–3% of the unsaturated contaminant is formed during the polymerization of the monomer. The presence of some agglomeration of PtRu NPs on PDDA-CNTs (Fig. 3a) indicate that the orbital overlap through π–π transition via the 2–3% unsaturated contaminant in the PDDA chain may not be sufficient to cover the whole surface of the CNTs, leading to the relatively lower density of PtRu NPs when compared with that PtRu supported on PEI and AP functionalized CNTs.

In the case of THF functionalized CNTs, THF interacts with the CNTs through the σ–π interaction between the π bonds of CNTs and the σ bonds of cyclopentanes of THF [35]. However, the interaction between THF and CNTs would be relatively weak due to the small molecular weight and the weak σ–π interaction. This may explain the fact that PtRu NPs supported on THF-CNTs have a relatively larger average particle size (3.28 nm) as compared with that supported on PDDA-CNTs, PEI-CNTs as well as AP-CNTs.

Fig. 5 is the XRD spectra of the as-synthesized PtRu catalysts supported on functionalized CNTs. The high peak near 2θ of 26° originates from the graphitic carbon of CNTs. The XRD results show the presence of broad diffraction peaks at 39.6° and 46.3°, which can be assigned to Pt(1 1 1) and Pt(2 0 0) and consistent with the face-centered cubic (fcc) structure of platinum [46]. No recognizable Ru hexagonal close-packed (hcp) structure or RuO_2 tetragonal phase was observed in all the samples, suggesting that Ru is most likely incorporated into the Pt fcc lattice and forms Pt-Ru bimetallic alloy [47]. For crystallite size less than 5 nm, the spread of measured intensities becomes so large that neighboring reflections Pt(1 1 1) and Pt(2 0 0) start overlapping in amplitude rather than intensity [48]. The XRD patterns show that PtRu supported on PDDA-CNTs, THF-CNTs and AO-CNTs have higher peaks of Pt(1 1 1), which indicate the increased crystallinity and relatively larger particle sizes of PtRu NPs supported on PDDA and THF functionalized CNTs. The relatively lower intensity and overlapping of the neighboring

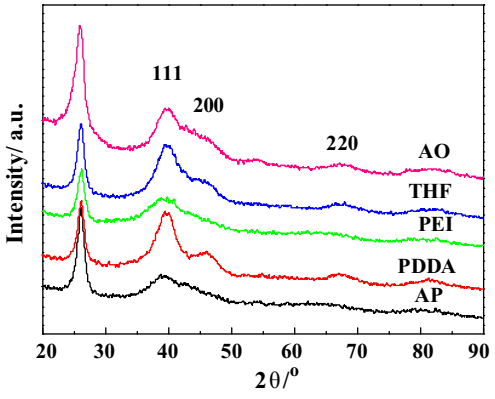

Fig. 5. XRD patterns of PtRu/PDDA-CNTs, PtRu/PEI-CNTs, PtRu/AP-CNTs, PtRu/THF-CNTs and AO-CNTs catalysts.

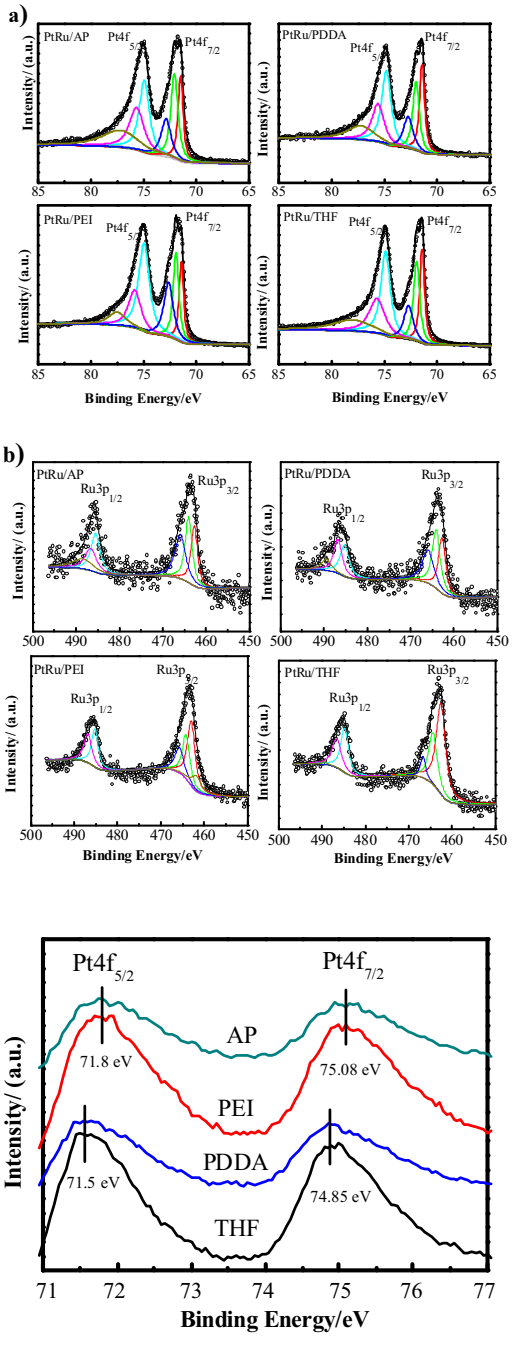

Fig. 6. XPS core-level spectra for Pt 4f and Ru 3p regions of PtRu/PDDA-CNTs, PtRu/PEI-CNTs, PtRu/AP-CNTs, and PtRu/THF-CNTs catalysts.

Table 2
ICP and XPS results of PtRu NPs supported on functionalized CNTs.

Species	Relative concentration (%)				Species	Relative concentration (%)			
	AP	PDDA	PEI	THF		AP	PDDA	PEI	THF
Pt(0)	42.3	43.3	44	44.2	Ru(0)	46.1	37.6	79.4	55.6
Pt(II)	32.4	32.4	33.8	32	Ru(IV)	35.2	36.8	10.3	33.3
Pt(IV)	25.3	24.1	22	23.9	Ru(IV) (hydrate)	18.7	25.6	10.3	11.1
	Pt:Ru ratio by ICP					Pt:Ru ratio by XPS			
	1.02:1	0.94:1	1.01:1	0.97:1		1.04:1	0.85:1	1.01:1	0.89:1
	Binding Energy (eV)					Binding Energy (eV)			
	AP	PDDA	PEI	THF		AP	PDDA	PEI	THF
Pt $4f_{7/2}$	75.08	74.85	75.08	74.85	Ru $3p_{3/2}$	485.8	486.5	485.8	485.2
Pt $4f_{5/2}$	71.8	71.5	71.8	71.5	Ru $3p_{1/2}$	463.5	464.2	463.5	463.1

reflections of Pt(1 1 1) and Pt(2 0 0) for PtRu NPs supported on PEI and AP functionalized CNTs indicates PtRu NPs supported on PEI and AP functionalized CNTs have a smaller average particle size, which are consistent with the results obtained from the TEM data.

XPS was employed to analyze the composition of PtRu supported on functionalized CNTs and the results are shown in Fig. 6 and Table 2. XPS peak deconvolution of Pt 4f and Ru 3p reveal metallic Pt(0), Pt(II) and Pt(IV) on the PtRu NPs on functionalized CNTs are in the range of 42.3–44.2%, 32–33.8% and 22–25.3%, respectively, indicating that the distribution of Pt(0), Pt(II) and Pt(IV) species is similar for the PtRu catalysts studied. However, the binding energy of Pt is affected by the functionalization agent. Pt 4f binding energy of PtRu NPs in PtRu/PEI-CNTs and PtRu/AP-CNTs shifted +0.23 eV as compared with that in PtRu/PDDA-CNTs and PtRu/THF-CNTs (Fig. 6c). The change of the binding energy of Pt 4f is most likely due to the electron transfer between Pt and amino groups in the PtRu/PEI-CNTs and PtRu/AP-CNTs catalysts, similar to that observed in Pt NPs supported on polypyrrole carbon black [49] and in Au clusters stabilized by poly(N-vinyl-2-pyrrolidone) [50]. In the case of Ru, there is more metallic Ru(0) observed for PtRu supported on PEI-CNTs (79.4%). Relatively high Ru(0) was also observed for PtRu supported on THF (55.6%) and AP (46.1%) functionalized CNTs. For PtRu/PDDA-CNTs; Ru(0) is of 37.6%.

As shown in Table 2, the Pt:Ru ratio obtained from XPS is 1.04:1, 0.85:1, 1.01:1 and 0.89:1 for PtRu supported on AP, PDDA, PEI and THF functionalized CNTs, respectively. The results show that PtRu supported on AP and PEI functionalized CNTs present an idea alloy surface with Pt:Ru ratio closing 1:1. The composition of Ru for PtRu supported on PDDA and THF functionalized CNTs is slightly higher than that obtained from ICP. Though the average NPs size of the prepared PtRu catalysts are in the range of 2.9–3.2 nm, the XPS results would enhance the composition of atoms in the surface region [51]. Thus the XPS data could be regarded as near-surface composition [51,52]. Hence, the concentration of Ru on the surface for PtRu NPs supported on PDDA and THF functionalized CNTs is slightly higher than Pt.

3.3. Electrocatalystic activity for CO stripping and methanol oxidation reaction

Fig. 7a is the cyclic voltammograms (CVs) for PtRu/CNTs catalysts in a nitrogen-saturated 0.5 M H_2SO_4 solution at a scan rate of 50 mV s^{-1}. The peaks in the potential region −0.2 to 0.1 V are associated with the hydrogen adsorption and desorption processes [53]. The coulombic charge for hydrogen desorption (Q_H) was used to calculate the electrochemical surface area (ESA) of the electrodes. The value of Q_H was calculated as the mean value between the amounts of charge exchanged during the electro-adsorption and desorption of H_2 on Pt sites minus the contribution of "double layer" charge. The values of ESA for PtRu NPs supported on PDDA, PEI, AP, THF and acid functionalized CNTs are 123.3, 141.4, 132.4, 126.2 and 62.3 $m^2\ g^{-1}{}_{Pt}$, respectively. The results indicate the ESA of PtRu supported on PDDA, PEI, AP and THF functionalized CNTs are quiet similar but more than 100% higher than that for PtRu NPs supported on AO-CNTs. The ESA of PtRu NPs supported on the functionalized CNTs is listed in Table 3.

Polyelectrolyte and solvent functionalization also enhances the activity of PtRu NPs for the CO oxidation reaction (Fig. 7b). In the case of PtRu/PEI-CNT and PtRu/AP-CNTs, the peak current density for CO oxidation is 335 and 306 mA $mg^{-1}{}_{Pt}$ with the similar onset potential at 0.35 V and peak potential of 0.59 and 0.63 V, respectively. On the other hand, the CO oxidation peak is positively shifted to a high potential (0.67 V) for PtRu/PDDA-CNTs. This may be because PDDA is able to draw electron from Pt atoms and increase the d-band center resulting in a strong chemisorption of CO species [37]. PtRu/THF-CNTs show relatively poor activity for CO

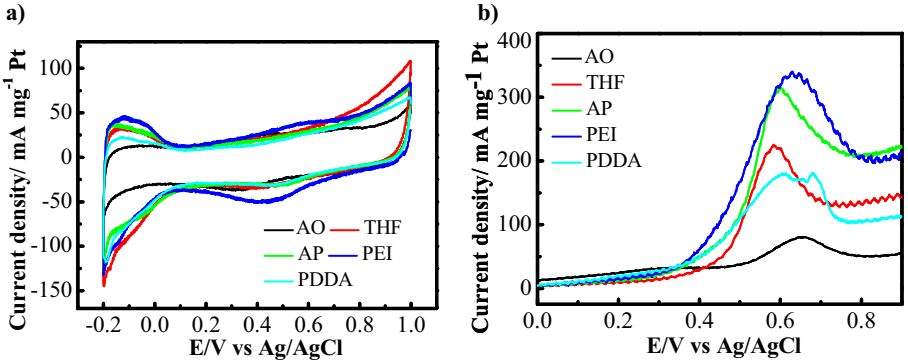

Fig. 7. Cyclic voltammograms of PtRu/PDDA-CNTs, PtRu/PEI-CNTs, PtRu/AP-CNTs, PtRu/THF-CNTs and PtRu/AO-CNTs (a) in a N_2-saturated 0.5 M H_2SO_4 and (b) in a CO-saturated 0.5 M H_2SO_4 solution. The scan rate was 50 mV s^{-1}.

Table 3
Particle size, electrochemical surface area (ESA), peak current density (j_p) and current density of PtRu supported on functionalized CNTs measured at different potentials for the methanol oxidation reaction.

Electrocatalysts	Particle size (nm)	ESA ($m^2\ g^{-1}{}_{Pt}$)	Onset potential (mV)	j_p ($mA\ mg^{-1}{}_{Pt}$)	Current density ($mA\ mg^{-1}{}_{Pt}$)		
					0.3 V	0.4 V	0.5 V
PDDA	3.13	123.3	250	440	115	182	214
PEI	2.98	141.4	200	635	152	291	375
AP	2.94	132.5	200	585	121	202	276
THF	3.28	126.2	250	425	105	158	195
AO	4.2	62.3	500	110	52	75	100

oxidation with an onset potential of 0.4 V and peak current density of 204 $mA\ mg^{-1}{}_{Pt}$ at ~0.58 V. The electrocatalytic activity of PtRu supported on AO-CNTs for CO oxidation is very poor, indicated by a low peak current density of 76 $mA\ mg^{-1}{}_{Pt}$ at 0.66 V.

Fig. 8 is the CVs for the MOR of PtRu NPs supported on functionalized CNTs in a 0.5 M H_2SO_4 + 1.0 M CH_3OH solution at scan rate of 50 $mV\ s^{-1}$, measured at scan potential windows of −0.2 to 1.0 V and −0.2 to 0.6 V, respectively. The electrocatalytic activity of the Pt based electrocatalysts can be assessed by the forward peak current density [22,36,54,55]. The peak current density for the MOR on PtRu/AO-CNTs is 110 $mA\ mg^{-1}{}_{Pt}$, significantly lower than that observed for the reaction on PtRu supported on non-covalent functionalized CNTs (Fig. 8a). This again demonstrates that non-covalent functionalized CNTs are better supports for PtRu NPs, consistent with the data reported elsewhere [22]. The best performance was obtained on PtRu NPs supported on PEI-CNTs and AP-CNTs, achieving a peak current of 635 and 585 $mA\ mg^{-1}{}_{Pt}$, which is significantly better than 440 and 425 $mA\ mg^{-1}{}_{Pt}$ measured on PtRu/PDDA-CNTs and PtRu/THF-CNTs, respectively.

The electrocatalytic activity of Pt-based electrodes for the MOR can also be assessed at potentials more appropriate to the actual working conditions of DMFCs [11,47,56]. In order to eliminate the possible complications due to the formation of Pt-oxides and catalyst degradation [11,57,58], the CVs were obtained with upper limit potential of 0.6 V (see Fig. 8b). The current densities measured at 0.3, 0.4 and 0.5 V show a similar dependence on the composition and structure of the functionalization agents, similar to that observed with the peak current density. For example, the current density at 0.4 V is 182, 291, 202, and 158 $mA\ mg^{-1}{}_{Pt}$ for PtRu supported on PDDA, PEI, AP and THF functionalized CNTs, which is significantly higher than 75 $mA\ mg^{-1}{}_{Pt}$ on PtRu/AO-CNTs. PtRu/PEI-CNTs have the highest current densities at the potential ranges measured in this study. The current densities measured at 0.3, 0.4 and 0.5 V and onset potential are also given in Table 3. The present study also indicates that both peak current densities and current densities measured at potential more appropriate for DMFCs can be used to assess the electrocatalytic activity of the Pt-based electrodes. However, a caution should be taken that if the activity is to be assessed at potentials more appropriate for fuel cell operation conditions, the linear or CV scan potential windows should be carefully controlled or selected.

Fig. 9 is the chronoamperometry curves of the PtRu NPs supported on functionalized CNTs, measured in a 0.5 M H_2SO_4 + 1.0 M CH_3OH solution at a constant potential of 0.6 V and 0.4 V, respectively. The oxidation current decrease rather rapidly initially for the catalysts studied and the decay is most likely due to the poisoning of intermediate species, such as CO_{ads}, CH_3OH_{ads}, $COOH_{ads}$, and CHO_{ads} formed during the methanol oxidation reaction [59,60]. In the case of the chronoamperometry curves measured at 0.6 V, PtRu/PEI-CNTs, PtRu/AP-CNTs and PtRu/PDDA-CNTs reached a relatively stable current density of 160, 106 and 80 $mA\ mg^{-1}{}_{Pt}$, respectively, after initial current decay. For the

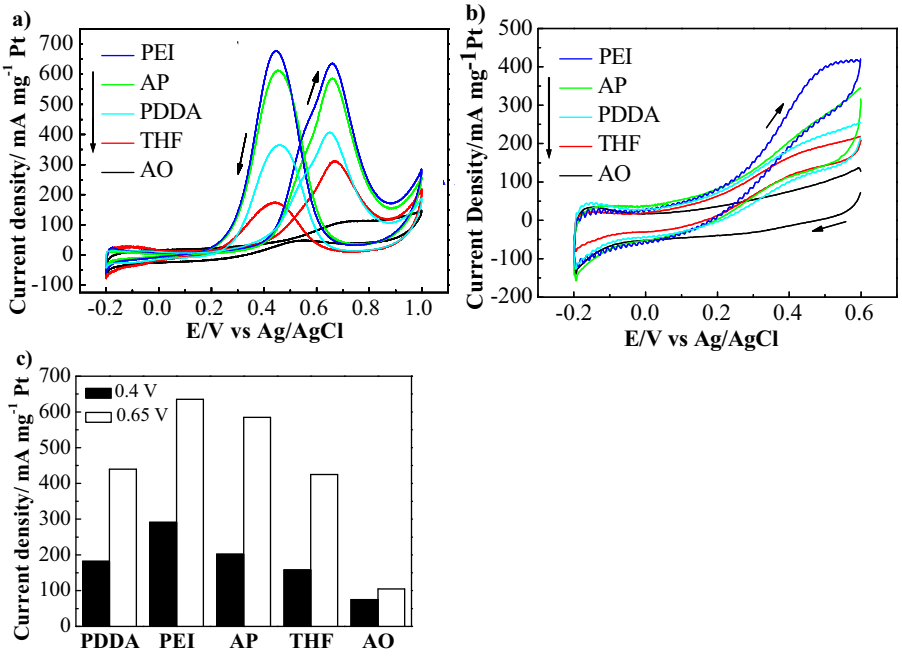

Fig. 8. Cyclic voltammograms of PtRu/PDDA-CNTs, PtRu/PEI-CNTs, PtRu/AP-CNTs, PtRu/THF-CNTs and PtRu/AO-CNTs in a N_2-saturated 0.5 M H_2SO_4 + 1.0 M CH_3OH solution, measured (a) from −0.2 to 1.0 V and (b) from −0.2 to 0.6 V. The scanning rate was 50 $mV\ s^{-1}$. Peak current density and current density at 0.4 V for the methanol oxidation are given in (c).

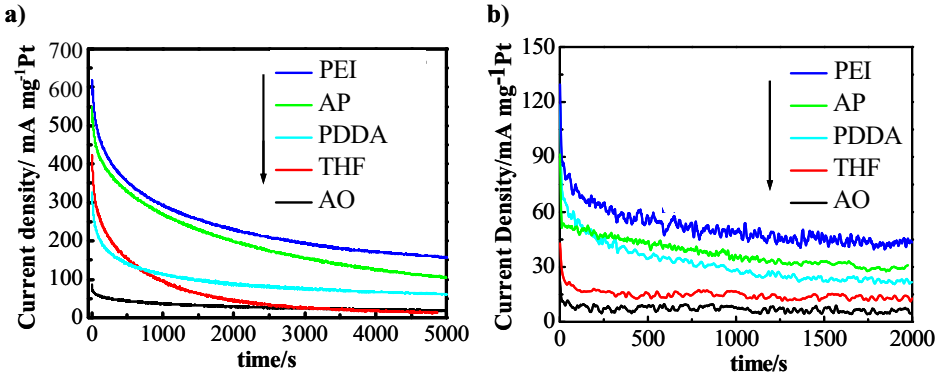

Fig. 9. Chronoamperometry curves of PtRu/PDDA-CNTs, PtRu/PEI-CNTs, PtRu/AP-CNTs, PtRu/THF-CNTs and PtRu/AO-CNTs measured in a 0.5 M H_2SO_4 + 1.0 M CH_3OH solution under a potential of (a) 0.6 V and (b) 0.4 V.

reaction on PtRu/THF-CNTs and PtRu/AO-CNTs, the current is 16 and 18 mA mg^{-1}_{Pt} after polarized for 5000 s. These results indicate that PtRu NPs supported on PEI, AP and PDDA functionalized CNTs have a much higher stability as compared to that on THF-CNTs and AO-CNTs.

For a practical methanol/O_2 fuel cell, the open circuit voltage (OCV) is ~0.8 V vs. RHE (~0.6 vs. Ag/AgCl) due to the methanol crossover from the anode to the cathode through the proton exchange membrane. For the methanol oxidation at the anode, the potential would be 0.5–0.7 vs RHE, which corresponds to 0.3–0.5 V vs. Ag/AgCl. Thus, it is also important to assess the stability of the Pt based electrocatalysts at potentials within the operation potentials of the electrodes under fuel cell operation conditions. Fig. 9b shows the chronoamperometry curves measured at 0.4 V. The polarization potential for the MOR shows a similar decay, as observed for that measured at 0.6 V. Moreover, the order of the stability of the PtRu supported on functionalized CNTs is more or less the same as that measured at 0.6 V. The PtRu/PEI-CNTs show the highest stability or tolerance towards the poisoning of the intermediate species of the MOR, achieving ~45 mA g^{-1}_{Pt} after polarized for 2000 s, substantially higher than ~12 and 7 mA g^{-1}_{Pt} obtained on PtRu/THF-CNTs and PtRu/AO-CNTs measured under identical conditions.

3.4. Effect of functionalization agents

The present study shows that the composition and structure of the functionalization agents play an important role in the electrocatalytic activity of PtRu NPs for the MOR. The much better dispersion and smaller particle size of PtRu supported on non-covalent functionalized CNTs by PDDA, PEI, AP and THF as compared to that supported on acid functionalized CNTs clearly indicates that non-covalent functionalization is very effective to introduce uniformly distributed binding sites on CNTs with no detrimental effect on the intrinsic properties of CNTs. The TGA and Raman analysis demonstrate that non-covalent functionalization also enhance the thermal stability of CNTs in particular for the functionalization agents with strong intermolecular force or interaction with the CNTs, e.g., through π–π stacking between the functionalization agents and CNTs. In the case of weak intermolecular force between the functionalization agent like THF and CNTs, the non-covalent functionalization enhances the dispersion of PtRu NPs but has little effect on the thermal stability of CNTs.

The significant benefit of the non-covalent functionalization is also supported by the much higher electrocatalytic activity of PtRu NPs supported on PDDA, PEI, AP and THF functionalized CNTs as compared to that on AO-CNTs (Fig. 8a). PtRu NPs supported on PEI, AP, PDDA and THF functionalized CNTs show a significantly higher peak current density (635–425 mA mg^{-1}_{Pt}) than 110 mA mg^{-1}_{Pt} measured on PtRu/AO-CNTs. The current density measured at potentials close to the fuel cell operation conditions for the reaction on PtRu NPs supported on PEI, AP, PDDA and THF functionalized CNTs is also significantly higher than that on PtRu/AO-CNTs (see Table 3). Most important observation in the present study is the significant dependence of the electrocatalytic stability of the PtRu NPs on the nature of the functionalization agents. The PtRu NPs on PDDA, PEI and AP functionalized CNTs show a much better stability (160–80 mA mg^{-1}_{Pt} at 0.6 V after polarized for 5000 s and 60–25 mA mg^{-1}_{Pt} at 0.4 V after polarized for 2000 s) as compared to that supported on THF-CNTs. For the reaction on PtRu/THF-CNTs, the current density is 16 mA mg^{-1}_{Pt} at 0.6 V and 12 mA mg^{-1}_{Pt} at 0.4 V at the end of the stability test, which is close to 18 and 7 mA mg^{-1}_{Pt} measured on PtRu/AO-CNTs under the same test conditions. This indicates that THF functionalization has no promotion effect on the tolerance of PtRu electrocatalysts towards the poisoning of the reaction intermediates. The best results were obtained on PtRu/PEI-CNTs with highest activity and stability for the methanol oxidation reaction (see Table 3). On the other hand, XPS analysis shows that the differences in the PtRu ratio or the electronic states of the PtRu NPs supported on functionalized CNTs are very small (Table 2).

PEI and AP contain amino groups while PDDA is a water-soluble quaternary ammonium polyelectrolyte. THF is an oxygen-containing heterocycle with five-membered rings and no nitrogen-containing groups. The electronegativity difference between carbon and oxygen makes the C—O bond moderately polar. PEI is a cationic polymer with repeating unit composed of the amine group and two carbon aliphatic CH_2CH_2 spacers (Fig. 1). The assembly of the PEI on CNTs would be strong due to the high molecular weight and the electrostatic attraction between the positively charged PEI and negatively charge CNTs, resulting in the attachment of large amount of N-containing amine group on the outer surface of CNTs. PDDA is also a cationic polymer with N-containing repeating unit, but the π–π interaction with the CNTs surface primarily occurs through the 2–3% of unsaturated contaminant in the PDDA chain [44,45]. This may limit the attachment of N-containing functional groups to the surface of CNTs. The lower density of attached N-groups on the CNTs surface may also contribute to the relatively poor dispersion of PtRu NPs on PDDA-CNTs (Fig. 4a). In the case of 1-AP, the interaction with CNTs is via π–π stacking. However, due to the bulk size of benzene rings, the attached nitrogen functional groups on the surface of CNTs would be expected to be smaller than that of PEI but higher than that of PDDA. Fig. 10 shows schematically the assembly of PEI, AP and PDDA on the outer wall surface of CNTs. The high density of N-containing functional groups assembled on CNTs in the case of PEI and AP is consistent with the +0.23 eV positive shift of Pt 4f BE of PtRu NPs supported on PEI and AP

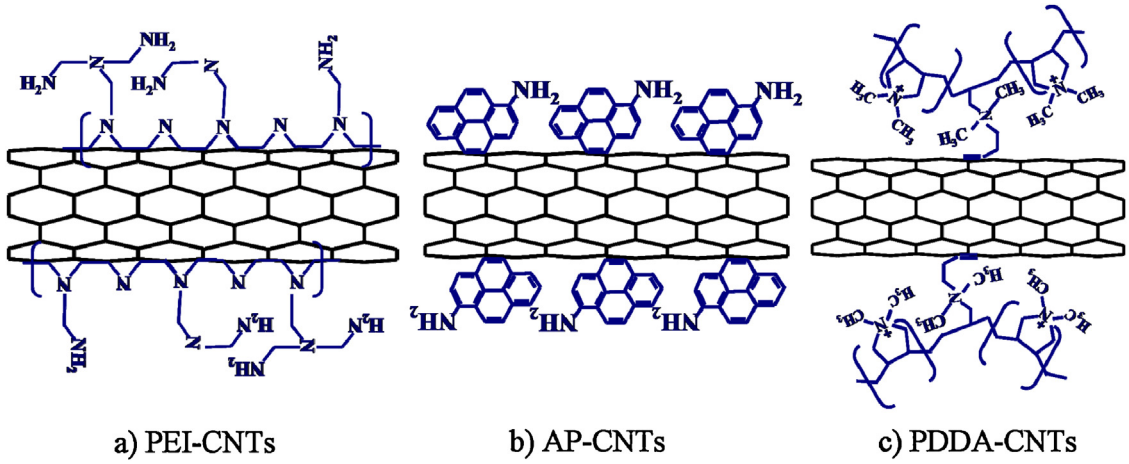

Fig. 10. Schematic of the assembly and functionalization of PEI, AP and PDDA on the surface of CNTs.

functionalized CNTs as compared to that supported on PDDA-CNTs (Fig. 6c).

It has been shown that the doped carbon materials by nitrogen, boron, phosphorus and sulfur have high electrocatalytic activity, high durability and high tolerance towards poisoning of the fuel cell reactions [61–65]. Doping with heteroatoms can modulate the structure, electronic and physicochemical properties of carbon materials like CNTs. For example, for the N-doped electron rich CNTs, the π electrons of carbon can be activated by the conjugation with the lone-pair electrons of N dopants, and the O_2 can be effectively reduced on the neighboring positively charged carbon atoms [66]. Nitrogen doped CNTs and graphene also enhance the activity of Pt and PtRu NPs for the MOR [67–69]. Incorporation of nitrogen into carbon supports also improve the stability of PtRu NPs for the MOR as shown by Olsen et al. [70]. The electron-rich dopants such as nitrogen are beneficial for the breaking the electroneutrality of the sp^2 carbon to create charged sites for the adsorption of oxygen species and promote the MOR and oxygen reduction reaction [49,71].

N-containing functionalization agents such as PEI and AP would have higher amino-containing functional groups assembled on the CNTs as compared with that of PDDA, as schematically shown in Fig. 10. The positive shift of the BE of Pt 4f in the case of PtRu NPs supported on PEI and AP functionalized CNTs indicates the strong interaction between N-containing functional groups assembled on CNTs and PtRu NPs, most likely due to the electron donating of large number of nitrogen-containing functional group assembled on CNTs. In the case of PDDA-CNTs, the electron donating effect of limited quaternary ammonium group assembled on the CNTs surface may be reduced by the electron drawing of cationic PDDA. This may explain the no change in the BE of Pt 4f for PtRu/PDDA-CNTs (Fig. 6c). The nitrogen in the amino functional groups of the attached functionalization agents can activate the π electrons of CNTs supports and promotes the MOR, similar to that observed for the N-doped carbon materials like CNTs and grapheme [66–69]. The promotion effect of nitrogen in the functionalization agents is evidently supported by the high activity and stability of PtRu supported on PEI and AP functionalized CNTs and in less degree on PDDA functionalized CNTs, as compared with THF and AO functionalized CNTs. The results in the present study indicate the strong dependence of the activity and stability of PtRu NPs on the distribution and density of N-containing functional groups assembled on the surface of CNTs in the following order:

PtRu/PEI-CNTs > PtRu/AP-CNTs > PtRu/PDDA-CNTs ≫ PtRu/THF-CNTs ~ PtRu/AO-CNTs.

THF contains no nitrogen and thus, despite the initial high activity of PtRu/THF-CNTs for the methanol oxidation reaction, its resistance toward the poisoning of intermediate species such as CO of the methanol oxidation reaction is very low as the assembled THF offers no promotion effect for the MOR, similar to that of PtRu/AO-CNTs (Fig. 9).

4. Conclusions

In this work, the effect of nitrogen-containing functionalization was studied on PtRu NPs supported on PDDA, PEI, AP and THF functionalized CNTs. PtRu NPs with particle size around 3 nm and similar Pt/Ru ratio were successfully synthesized onto the functionalized CNTs. Non-covalent functionalization by polyelectrolytes or solvents is far more effective to uniformly assembly PtRu NPs on CNTs and enhances the thermal and structural stability of CNTs as compared with the conventional acid functionalized CNTs. PtRu catalysts supported on PEI-CNTs and AP-CNTs and in less extent on PDDA-CNTs exhibited much higher electrocatalytic activity and stability toward the MOR as compared to that on THF-CNTs and AO-CNTs. The fundamental reason for the high electrocatalytic activity of PtRu NPs on PEI, AP and in less extend on PDDA functionalized CNTs is the strong interaction between the electron rich nitrogen of the functional group of the functionalization agents and CNTs, indicated by the positive shift of the BE of Pt 4f. The strong interaction of electron-rich nitrogen of the functional groups could activate the π electrons of carbon and promote the electrocatalytic activity and stability of PtRu catalysts, similar to that reported on nitrogen-doped carbon materials. The results indicate that the functionalization agents with ammonium or amino groups are particularly effective to enhance the activity of the PtRu NPs for the methanol oxidation reaction of fuel cells. The present study also indicates that both peak current densities and current densities measured at potentials more appropriate for fuel cell operation conditions can be used to assess the electrocatalytic activity of the Pt-based electrocatalysts for fuel cells.

Acknowledgements

This work was supported by the Australian Research Council *Discover Project funding scheme* (project number: DP120102325 & DP120104932) and the Major International (Regional) Joint Research Project of NNSFC (51210002), China. The authors acknowledge the facilities, scientific and technical assistance of the Curtin University Electron Microscope Facility and Curtin X-Ray

Laboratory, both of which are partially funded by the University, State and Commonwealth Governments.

References

[1] X. Zhao, M. Yin, L. Ma, L. Liang, C. Liu, J. Liao, T. Lu, W. Xing, Energy Environ. Sci. 4 (2011) 2736–2753.
[2] Y.L. Hsin, K.C. Hwang, C.-T. Yeh, J. Am. Chem. Soc. 129 (2007) 9999–10010.
[3] L.H. Jiang, G.Q. Sun, X.S. Zhao, Z.H. Zhou, S.Y. Yan, S.H. Tang, G.X. Wang, B. Zhou, Q. Xin, Electrochim. Acta 50 (2005) 2371–2376.
[4] C.M. Zhou, F. Peng, H.J. Wang, H. Yu, C. Peng, J.A. Yang, Electrochem. Commun. 12 (2010) 1210–1213.
[5] Y.C. Zou, X. Li, Y.M. Huang, H.L. Liu, Chem. J. Chin. Univ.-Chin. 32 (2011) 150–154.
[6] K. Sundmacher, Ind. Eng. Chem. Res. 49 (2010) 10159–10182.
[7] C. Hu, Y. Cao, L. Yang, Z. Bai, Y. Guo, K. Wang, P. Xu, J. Zhou, Appl. Surf. Sci. 257 (2011) 7968–7974.
[8] O. Guillen-Villafuerte, R. Guil-Lopez, E. Nieto, G. Garcia, J.L. Rodriguez, E. Pastor, J.L.G. Fierro, Int. J. Hydrogen Energy 37 (2012) 7171–7179.
[9] V. Neburchilov, J. Martin, H. Wang, J. Zhang, J. Power Sources 169 (2007) 221–238.
[10] A. Chen, P. Holt-Hindle, Chem. Rev. 110 (2010) 3767–3804.
[11] F.A. Viva, M.M. Bruno, M. Jobbagy, H.R. Corti, J. Phys. Chem. C 116 (2012) 4097–4104.
[12] C. Arbizzani, S. Beninati, F. Soavi, A. Varzi, M. Mastragostino, J. Power Sources 185 (2008) 615–620.
[13] M. Tsuji, M. Kubokawa, R. Yano, N. Miyamae, T. Tsuji, M.-S. Jun, S. Hong, S. Lim, S.-H. Yoon, I. Mochida, Langmuir 23 (2006) 387–390.
[14] J. Prabhuram, T.S. Zhao, Z.K. Tang, R. Chen, Z.X. Liang, J. Phys. Chem. B 110 (2006) 5245–5252.
[15] Y. Kuang, Y. Cui, Y. Zhang, Y. Yu, X. Zhang, J. Chen, Chem.-a Eur. J. 18 (2012) 1522–1527.
[16] D. Eder, Chem. Rev. 110 (2010) 1348–1385.
[17] Q. Zhang, J.-Q. Huang, W.-Z. Qian, Y.-Y. Zhang, F. Wei, Small 9 (2013) 1237–1265.
[18] M.A. Herrero, M. Prato, Mol. Cryst. Liquid Cryst. 483 (2008) 21–32.
[19] B.H. Wu, D. Hu, Y.J. Kuang, Y.M. Yu, X.H. Zhang, J.H. Chen, Chem. Commun. 47 (2011) 5253–5255.
[20] Z.Q. Tian, S.P. Jiang, Y.M. Liang, P.K. Shen, J. Phys. Chem. B 110 (2006) 5343–5350.
[21] C.Y. Hu, Y.J. Xu, S.W. Duo, R.F. Zhang, M.S. Li, J. Chin. Chem. Soc. 56 (2009) 234–239.
[22] S.Y. Wang, X. Wang, S.P. Jiang, Langmuir 24 (2008) 10505–10512.
[23] S. Wang, S.P. Jiang, X. Wang, Nanotechnology 19 (2008).
[24] K.R. Reddy, B.C. Sin, K.S. Ryu, J.-C. Kim, H. Chung, Y. Lee, Synth. Met. 159 (2009) 595–603.
[25] Y. Cheng, S.P. Jiang, Electrochim. Acta 99 (2013) 124–132.
[26] H.-Y. Lee, W. Vogel, P.P.-J. Chu, Langmuir 27 (2011) 14654–14661.
[27] N.C. Cheng, S.C. Mu, X.J. Chen, H.F. Lv, M. Pan, P.P. Edwards, Electrochim. Acta 56 (2011) 2154–2159.
[28] G.N. Ostojic, J.R. Ireland, M.C. Hersam, Langmuir 24 (2008) 9784–9789.
[29] S. Wang, X. Wang, S.P. Jiang, Phys. Chem. Chem. Phys. 13 (2011) 7187–7195.
[30] D. Wang, S. Lu, S.P. Jiang, Chem. Commun. 46 (2010) 2058–2060.
[31] V. Selvaraj, M. Alagar, Electrochem. Commun. 9 (2007) 1145–1153.
[32] Y.C. Zhao, X.L. Yang, J.N. Tian, F.Y. Wang, L. Zhan, J. Power Sources 195 (2010) 4634–4640.
[33] J. Li, W. Yang, H. Zhu, X.L. Wang, F. Yang, B.L. Zhang, X.R. Yang, Talanta 79 (2009) 935–939.
[34] Z. Bai, Y. Guo, L. Yang, L. Li, W. Li, P. Xu, C. Hu, K. Wang, J. Power Sources 196 (2011) 6232–6237.
[35] D. Wang, S. Lu, S.P. Jiang, Electrochim. Acta 55 (2010) 2964–2971.
[36] S.Y. Wang, S.P. Jiang, T.J. White, J. Guo, X. Wang, J. Phys. Chem. C 113 (2009) 18935–18945.
[37] S. Wang, F. Yang, S.P. Jiang, S. Chen, X. Wang, Electrochem. Commun. 12 (2010) 1646–1649.
[38] J. Li, W. Yang, H. Zhu, X. Wang, F. Yang, B. Zhang, X. Yang, Talanta 79 (2009) 935–939.
[39] S.-C. Yi, C.Y. Jung, W.J. Kim, Mater. Res. Bull. 46 (2011) 2433–2440.
[40] Z. Lin, L. Ji, W.E. Krause, X. Zhang, J. Power Sources 195 (2010) 5520–5526.
[41] U.J. Kim, C.A. Furtado, X.M. Liu, G.G. Chen, P.C. Eklund, J. Am. Chem. Soc. 127 (2005) 15437–15445.
[42] G. Zhang, S. Sun, D. Yang, J.-P. Dodelet, E. Sacher, Carbon 46 (2008) 196–205.
[43] Y.-C. Chiang, W.-H. Lin, Y.-C. Chang, Appl. Surf. Sci. 257 (2011) 2401–2410.
[44] D.-Q. Yang, J.-F. Rochette, E. Sacher, J. Phys. Chem. B 109 (2005) 4481–4484.
[45] C. Caddeo, C. Melis, L. Colombo, A. Mattoni, J. Phys. Chem. C 114 (2010) 21109–21113.
[46] E. Antolini, F. Cardellini, J. Alloys Compounds 315 (2001) 118–122.
[47] M.L. Lin, M.Y. Lo, C.Y. Mou, J. Phys. Chem. C 113 (2009) 16158–16168.
[48] E.A. Baranova, Y. Le Page, D. Ilin, C. Bock, B. MacDougall, P.H.J. Mercier, J. Alloys Compounds 471 (2009) 387–394.
[49] S. Zhang, H. Wang, N. Zhang, F.D. Kong, H. Liu, G.P. Yin, J. Power Sources 197 (2012) 44–49.
[50] H. Tsunoyama, N. Ichikuni, H. Sakurai, T. Tsukuda, J. Am. Chem. Soc. 131 (2009) 7086–7093.
[51] F. Bensebaa, N. Patrito, Y. Le Page, P. L'Ecuyer, D. Wang, J. Mater. Chem. 14 (2004) 3378–3384.
[52] K.C. Park, I.Y. Jang, W. Wongwiriyapan, S. Morimoto, Y.J. Kim, Y.C. Jung, T. Toya, M. Endo, J. Mater. Chem. 20 (2010) 5345–5354.
[53] A. Pozio, M. De Francesco, A. Cemmi, F. Cardellini, L. Giorgi, J. Power Sources 105 (2002) 13–19.
[54] Y.J. Gu, W.T. Wong, Langmuir 22 (2006) 11447–11452.
[55] H.P. Cong, X.C. Ren, S.H. Yu, Chemcatchem 4 (2012) 1555–1559.
[56] K.W. Park, J.H. Choi, K.S. Ahn, Y.E. Sung, J. Phys. Chem. B 108 (2004) 5989–5994.
[57] L.R. Merte, F. Behafarid, D.J. Miller, D. Friebel, S. Cho, F. Mbuga, D. Sokaras, R. Alonso-Mori, T.C. Weng, D. Nordlund, A. Nilsson, B.R. Cuenya, Acs Catal. 2 (2012) 2371–2376.
[58] H. Popke, E. Mutoro, B. Luerssen, J. Janek, J. Phys. Chem. C 116 (2012) 1912–1920.
[59] T.H.M. Housmans, A.H. Wonders, M.T.M. Koper, J. Phys. Chem. B 110 (2006) 10021–10031.
[60] P. Ferrin, M. Mavrikakis, J. Am. Chem. Soc. 131 (2009) 14381–14389.
[61] Y.G. Chen, J.J. Wang, H. Liu, M.N. Banis, R.Y. Li, X.L. Sun, T.K. Sham, S.Y. Ye, S. Knights, J. Phys. Chem. C 115 (2011) 3769–3776.
[62] D.C. Higgins, D. Meza, Z.W. Chen, J. Phys. Chem. C 114 (2010) 21982–21988.
[63] D.S. Yu, Q. Zhang, L.M. Dai, J. Am. Chem. Soc. 132 (2010) 15127–15129.
[64] Y. Zheng, Y. Jiao, L. Ge, M. Jaroniec, S.Z. Qiao, Angew. Chem.-Int. Ed. 52 (2013) 3110–3116.
[65] M.S. Saha, R.Y. Li, X.L. Sun, S.Y. Ye, Electrochem. Commun. 11 (2009) 438–441.
[66] B. Shan, K. Cho, Chem. Phys. Lett. 492 (2010) 131–136.
[67] R. Chetty, S. Kundu, W. Xia, M. Bron, W. Schuhmann, V. Chirila, W. Brandl, T. Reinecke, M. Muhler, Electrochim. Acta 54 (2009) 4208–4215.
[68] G. Wu, R. Swaidan, D. Li, N. Li, Electrochim. Acta 53 (2008) 7622–7629.
[69] B. Xiong, Y.K. Zhou, Y.Y. Zhao, J. Wang, X. Chen, R. O'Hayre, Z.P. Shao, Carbon 52 (2013) 181–192.
[70] T.S. Olson, A.A. Dameron, K. Wood, S. Pylpenko, K.E. Hurst, S. Christensen, J.B. Bult, D.S. Ginley, R. O'Hayre, H. Dinh, T. Gennett, J. Electrochem. Soc. 160 (2013) F389–F394.
[71] T. Maiyalagan, B. Viswanathan, U. Varadaraju, Electrochem. Commun. 7 (2005) 905–912.